Self-Interfering Wave Packets

David Colas[1] and Fabrice P. Laussy[2,1,*]
[1]Departamento de Física Teórica de la Materia Condensada and Condensed Matter Physics Center (IFIMAC), Universidad Autónoma de Madrid, E-28049 Madrid, Spain
[2]Russian Quantum Center, Novaya 100, 143025 Skolkovo, Moscow Region, Russia
(Received 11 July 2015; revised manuscript received 5 October 2015; published 13 January 2016)

We study the propagation of noninteracting polariton wave packets. We show how two qualitatively different concepts of mass that arise from the peculiar polariton dispersion lead to a new type of particlelike object from noninteracting fields—much like self-accelerating beams—shaped by the Rabi coupling out of Gaussian initial states. A divergence and change of sign of the diffusive mass results in a "mass wall" on which polariton wave packets bounce back. Together with the Rabi dynamics, this yields propagation of ultrafast subpackets and ordering of a spacetime crystal.

DOI: 10.1103/PhysRevLett.116.026401

Field theory unifies the concepts of waves and particles [1]. In quantum physics, this brought to rest the dispute of the pre-second-quantization era, on the nature of the wave function. As one highlight of this conundrum, the coherent state emerged as an attempt by Schrödinger to prove to Heisenberg that his equation is suitable to describe particles since some solutions exist that remain localized [2]. However, the reliance on an external potential and the lack of other particle properties—like resilience to collisions—makes this qualification a moot point and quantum particles are now understood as excitations of the field. The deep connection between fields and particles is not exclusively quantum and classical fields also provide a robust notion of particles, most famously with solitons [3]. The particle cohesion is here assured self-consistently by the interactions, allowing free propagation and surviving collisions with other solitons (possibly with a phase shift). For a long time, this has been the major example of how to define a particle out of a classical field, until Berry and Balázs (an assistant of Schrödinger himself) discovered the first case of a similar behavior in a noninteracting context: the Airy beams [4]. These solutions to the Schrödinger equation (or, equivalently, through the Eikonal approximation, to Maxwell equations) retain their shape as they propagate as a train of peaks (or subpackets) and also exhibit self-healing after passing through an obstacle [5]. The ingredient powering these particle behaviors is phase shaping, assuring the cohesion by the acceleration of the subpackets inside the mother packet. The solution was first regarded as a mathematical curiosity as it is not normalizable, until a truncated version was experimentally realized and shown to exhibit this dramatic phenomenology but for a finite time [6]. The Airy beam is now a recognized particlelike object, in some cases emerging from fields that quantize elementary particles [7], thus behaving like a metaparticle. It is in fact but one example of a full family of so-called "accelerating beams" [8], that all similarly endow linear fields with particle properties: shape preservation and resilience to collisions.

In this Letter, we add another member to the family of mechanisms that provide noninteracting fields with particle properties. Namely, we show that two coupled fields of different masses can support self-interfering wave packets, resulting in the propagation of a train of subpackets, much like the Airy beam, but without acceleration, fully normalizable and self-created out of a Gaussian initial state. Such coupled fields can be conveniently provided in the laboratory by polaritons [9], the superposition of light $\psi_C(x,t)$ and matter fields $\psi_X(x,t)$, cf. Fig. 1. They find their most versatile and tunable implementation in semiconductors where excitons (electron-hole pairs) of a quantum well are coupled to microcavity photons. Dispersions can furthermore be tuned by light-matter engineering, e.g., with photonic crystal polaritons [10]. Since polaritons can form condensates with a wave function describing their

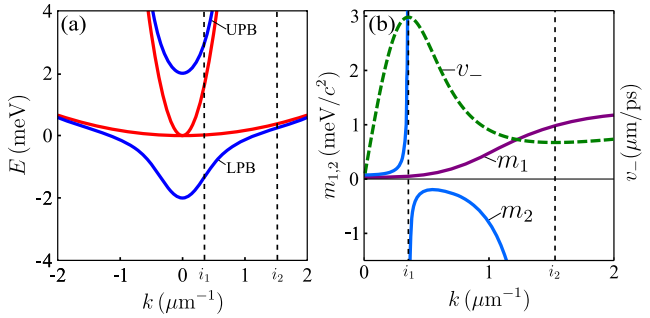

FIG. 1. (a) Polariton dispersions. In red: the parabolic dispersion of the cavity photon, and the bare exciton. In blue: the polariton branches $E_\pm$. The vertical dashed lines at i_1 and i_2 mark the inflection points of the LPB. Parameters: $\Omega_R = 2$ meV, $m_C = 0.025$ meV ps^2 μm^{-2}, $m_X = 2$ meV ps^2 μm^{-2}. (b) Effective masses for the LPB as a function of k: inertial mass m_1 (purple), diffusive mass m_2 (blue, negative when $i_1 < k < i_2$), and group velocity v_- (green).

collective dynamics [11], they are a dream laboratory to investigate the wave packet propagation in a variety of contexts [12], such as propagation of spin [13], bullets [14], or Rabi oscillations [15] with technological applications already in sight [16,17]. Polaritons are highly valued for their nonlinear properties due to particles' self-interactions [18], illustrated by a whole family of solitons (bright, dark, composite…) [19–22]. Recently, however, also the noninteracting regime has proved to be topical, with reports of Skyrmion analogues [23], band structure engineering [24] focusing and conical diffraction [25], Bosonic Josephson junctions [26], emulates of oblique dark and half solitons [27], topological edge modes [28,29], or the implementation of Hebbian learning in neural networks [30] to name a few but illustrative examples. In most of these cases, interactions bring the physics to even farther extents rather than spoiling the underlying linear effect, that remains nevertheless the one capturing the phenomenon. The linear regime can be achieved at low densities [31] since the polariton interaction at the few-particles level is small. The dynamics of the wave function $|\psi\rangle$ is then ruled by the polariton propagator Π such that $|\psi(t)\rangle = \Pi(t-t_0)|\psi(t_0)\rangle$. In free space, it is diagonal in k space [18]:

$$\langle k'|\Pi(t)|k\rangle = \exp\left[-i\begin{pmatrix} \frac{\hbar k^2}{2m_C}+\Delta & \Omega_R \\ \Omega_R & \frac{\hbar k^2}{2m_X}\end{pmatrix}t\right]\delta(k-k'), \quad (1)$$

where $m_{C,(X)}$ is the photon (exciton) mass, Δ their detuning, and Ω_R their Rabi coupling. The eigenstates of the propagator, $\Pi(t)||k\rangle\rangle_\pm = \exp(-iE_\pm t)||k\rangle\rangle_\pm$, define both the polariton dispersion $E_\pm = \hbar k^2 m_+ + 2\Delta \mp k_\Omega^2$ and the canonical polariton basis $||k\rangle\rangle_\pm \propto [E_\pm(k),1]^T|k\rangle$, where $m_\pm = (m_C \pm m_X)/(m_C m_X)$ are the reduced relative masses, $k_\Omega = \sqrt[4]{\hbar^2k^4m_-^2 - 4\hbar k^2\Delta m_- + 4(\Delta^2+4\Omega_R^2)}$ the dressed momentum and $|k\rangle$ the plane wave of well-defined momentum k. We use the notation $||\rangle\rangle_\pm$ for upper $(+)$ and lower $(-)$ polaritons. A general polariton state is thus expressed as $||\psi\rangle\rangle_\pm = \int_{-\infty}^{\infty}\phi_\pm(k)||k\rangle\rangle_\pm dk$, where $\phi_\pm(k)$ is the scalar-field polariton wave function. Except for a well-defined polariton state in k space, i.e., a fully delocalized polariton in real space, the photon and exciton components of a polariton cannot be jointly defined by a given wave packet $\phi(k)$. Indeed, except if $\phi(k)=\delta(k)$, one component gets modulated by the $E_\pm(k)$ factor needed to maintain the particle on its branch. One consequence of this composite structure is that a polariton cannot be localized in real space, with both its photon and exciton components simultaneously localized. Choosing $\phi(k)$ such that either $\psi_C(x,t=0)$ or $\psi_X(x,t=0)$ is $\delta(x)$ smears out the other component around the localized field, as shown in Figs. 2(a)–2(b). Such constraints result in a rich phenomenology with a large enough set of momenta. We now discuss some of the effects that arise from self-shaping and self-interferences of polaritons due to their composite structure.

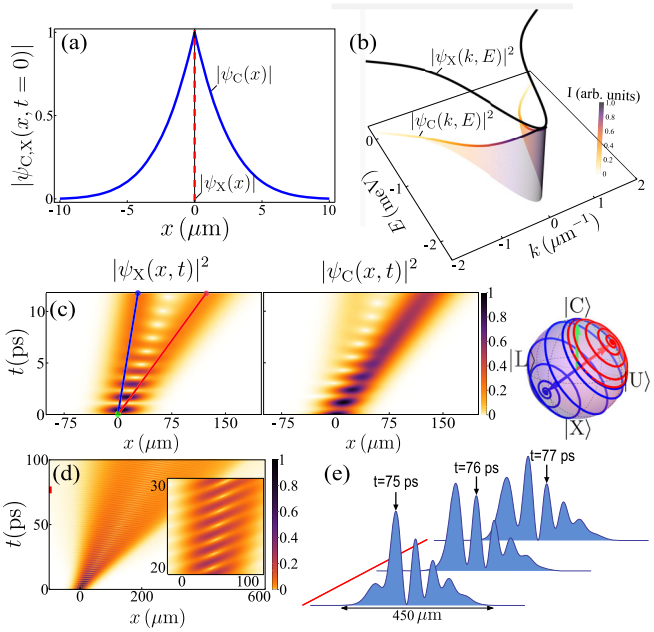

FIG. 2. (a) Localizing a polariton in space is possible for one of its component only (here in dashed red); the other field smears out to keep the particle on its branch. (b) Counterpart of (a) in energy-momentum space. (c) Spacetime evolution of $|\psi_C(x,t)|^2$ and $|\psi_X(x,t)|^2$ with a photon of momentum $k_0 = 0.5/\mu$m as an initial condition, with quantum states along the lines shown on the Bloch sphere. (d) Configuration with $\Delta = -\Omega_R$, preventing splitting of the beam and resulting in ultrafast, Rabi-powered, propagating subpackets, as shown for three snapshots of time in (e).

It has long been known that the mass imbalance $m_C \ll m_X$ results in peculiar dispersions for the upper (E_+) and lower (E_-) polariton branches, shown in Fig. 1(a) along with the parabolic dispersions of the light photon and the heavy exciton, meeting at $k=0$ $(\Delta=0)$. In order to provide a comprehensive picture including the two inflection points that can result for the lower polariton branch (LPB), we assume here a smaller mass ratio than in typical experiments. The most important effects are, however, due to the first inflection point that is found in most samples. To access more inflection points, one can also turn to other platforms such as modulated photonic lattices [32], crystals [10], or coupled wave guides [33] (we refer to the Supplemental Material [34] for further discussion and experimental implementations with currently available systems). The dynamics of a Gaussian wave packet large enough in space to probe only parabolic portions of the dispersion in reciprocal space is essentially that expected from Schrödinger dynamics [35], diffusing with mean standard deviation of the packet size [34]:

$$\sigma_x(t) = \sqrt{\sigma_x^2(0) + (\hbar t/[2m_2\sigma_x(0)])^2}. \quad (2)$$

For nonparabolic dispersions, the degeneracy is lifted for some of the various concepts of masses, famously unified for the gravitational and inertial masses by Einstein as part

of his theory of gravitation. Wave packets have two different effective masses, m_1 and m_2 [36], describing, respectively, propagation and diffusion. A wave packet propagates with a group velocity $v_\pm = \partial_k E_\pm(k)$. This defines the *inertial* mass m_1 that determines the wave packet velocity from de Broglie's relation $p = \hbar k$ and the classical momentum $p = m v_\pm$ as

$$m_1(E,k) = \hbar^2 k (\partial_k E)^{-1}. \quad (3)$$

A second mass m_2, that we will call the *diffusive* mass, is associated with the spreading of the wave packet according to Eq. (2) and depends on the branch's curvature; it reads

$$m_2(E,k) = \hbar^2 (\partial_k^2 E)^{-1}. \quad (4)$$

These two masses m_1, m_2, and the packet velocity v_- are plotted in Fig. 1(b) for the LPB. Unlike parabolic dispersions, where they are equal, polariton dispersions yield different inertial and diffusive masses. In particular, the k-dependent inertial mass m_1 imposes a maximum speed for the lower polaritons [34]. Beyond the inflection point i_1, polaritons slow down with increasing momentum (at large k, polaritons become bare particles with no such kinematic restrictions). The coupling of the two fields with different masses results in the heavier one lagging behind the other, as seen in Fig. 2(c) where a Gaussian photon wave packet is imparted with a momentum $k = 0.5/\mu$m, achieved experimentally by sending a pulse at an angle and overlapping both branches. This prevents the photon and exciton packets to propagate Rabi oscillating, and instead forces a splitting in two beams—the orthogonal polariton states which are eigenstates for the corresponding wave vector, as shown by their trajectory on the Bloch sphere—connected by a Rabi oscillating tunnel. The Rabi oscillations only take place when there is a spatial overlap between the polaritons. The two propagating packets maintain their coherence despite their space separation and would Rabi oscillate if meeting again, due, for instance, to a ping-pong reflection [37]. The splitting in two beams can be minimized by tuning parameters to equalize the polaritons masses, in particular, the inertial ones. Combined with the bending of the Rabi oscillations in spacetime, which can be achieved at nonzero detuning, this leads to propagation of Rabi oscillations, which produce ultrafast subpackets moving inside a mother packet, as shown in Fig. 2(d) and for three time snapshots in 2(e). The subpackets, continuously formed in the tail of the mother packet, propagate inside 1 order of magnitude faster, powered by Rabi oscillations, before dying in the head. Each subpeak acquires properties of an identifiable object, traceable in time. The full dynamics is available in an accompanying video [34]. Now on the diffusive mass m_2: it diverges at the two inflection points $i_{1,2}$ of the LPB and is negative in between. Exciting at the inflection points thus cancels diffusion as seen in Eq. (2) and in Figs. 3(a) and 3(b) with the propagation of a broad [$\sigma_x(0) = 20$ μm] lower-polariton wave packet with an imparted momentum of (a) $k_0 = 0$ and (b) $k_0 = i_1$. The excitation around the inflection point has already been used to generate bright solitons and soliton trains [19,20,38,39]. In these cases, the soliton mechanism is the interplay between negative effective mass and repulsive interactions. The role of the high effective mass close to the inflection point, which cancels the diffusion, was not, however, fully estimated.

The interesting phenomenology discussed so far illustrates isolated features of polariton propagation. A new physical picture emerges when combining several aspects within the same wave function, leading to the concept of

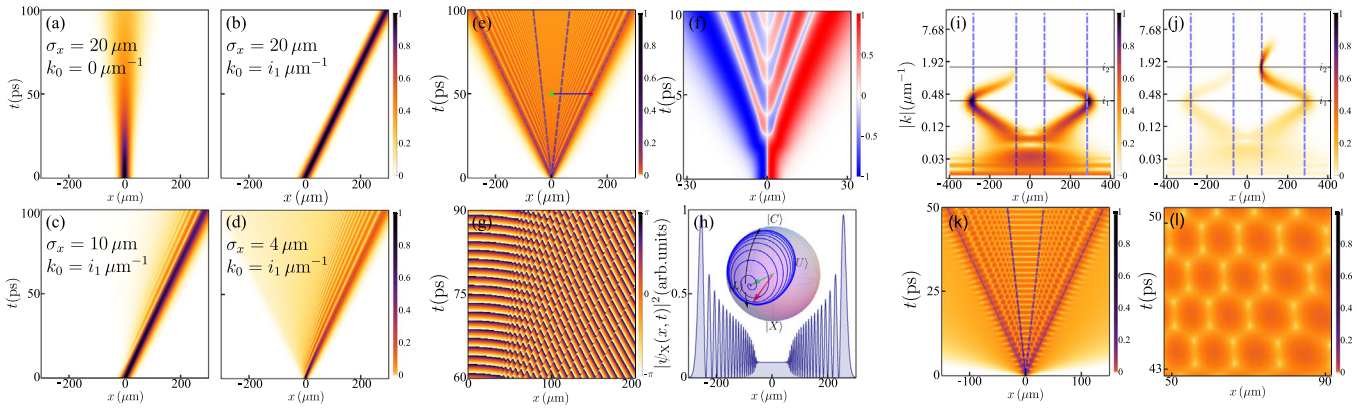

FIG. 3. (a)–(d) Propagation of lower polariton packets for various momenta and size, showing the emergence of the SIP for narrower packets. (e) Dynamics of an even narrower packet [$\sigma_x(0) = 2$ μm with no momentum $k_0 = 0$]. (f) Current probability j at early times, showing the coexistence and interleaving of net counterpropagating flows. (g) Phase map in a selected region, showing π jumps associated to each subpeak. (h) Intensity profile at $t = 90$ ps with the evolution of the quantum state on the Bloch sphere corresponding to the path (from green to red) plotted in (e). (i) Wavelet decomposition of (e) at $t = 100$ ps, and (j) in the same configuration but exciting with a momentum $k_0 = i_2$. (k) Spacetime honeycomb lattice when combining the SIP with Rabi oscillations by starting with a photon as an initial condition. (l) Zoom of the hexagonal lattice.

self-interfering packets (SIP). This occurs when reducing the wave packet size in real space, that is, increasing the staggering on the dispersion in momentum-space $[\sigma_k(0) = 1/\sigma_x(0)]$, to an extent enough to probe polaritonic deviation from the parabolic dispersion. In this case, the negative mass plays an explicit role. Negative masses are a recurrent theme in physics but this is typically meant for the inertial mass [40]. The sign of the diffusive mass would seem not to play a role since it is squared in Eq. (2), and this is indeed the case for momenta $i_1 < k < i_2$. When straddling over the divergence, however, self-interferences occur between harmonics of the packet subject to the positive mass and others to the negative mass. This results in a reshaping of the wave function, as shown in Figs. 3(c) and 3(d) decreasing $\sigma_x(0)$ down to 10 and 4 μm. The part of the packet that goes beyond the divergence is reflected back and interferes with the rest that still propagates forward, resulting in ripples. Reducing the packet to $\sigma_x(0) = 2$ μm produces the striking pattern seen in Fig. 3(e), without even imparting momentum. While for a parabolic dispersion, squeezing the packet in space merely causes a faster diffusion, in the polariton case, there is thus a critical diffusion beyond which the packet stops expanding and folds back onto itself. Since this happens when the wave function encounters the inflection point of the LPB, there is a "mass wall" against which the packet bounces back. If the dispersion also features another inflection point at larger k, this reflection happens again, shielding the core of the mother packet from this self-interference, as shown on the cut in intensity in Fig. 3(h) [the diffusion cones are the solution of $\partial_k^2 E_- = 0$, cf. Fig. 3(e)]. More importantly from a conceptual point of view, as a result of this coexistence of masses of opposite signs within the same packet, the mother wave packet $|\psi\rangle$ fragments itself into two trains of daughter shape-preserving subpackets traveling in opposite directions. The overall momentum $\langle\psi|p|\psi\rangle = 0$ is null but the self-shaping of the wave function redistributes it through its subpackets with nonzero momenta. Each subpeak can be identified as a polariton lying onto the meridian between $|L\rangle$ and $|X\rangle$, as seen by following its quantum state on the Bloch sphere, Fig. 3(h). The SIP can therefore be seen as a train of successive polariton packets, "emitted" at the rate of Rabi oscillations by the area shielded from self-interferences, retaining their individuality as they propagate inside the mother packet. The quantum state dynamics along these paths is seen vividly in a video in the Supplemental Material [34]. Successive peaks furthermore feature a maximal phase shift of π in the phase $\phi(x,t)$ of the total wave function $\psi(x,t) = |\psi(x,t)|\exp[i\phi(x,t)]$, as shown in Fig. 3(g). Although they do not involve self-interactions to account for their cohesion, these propagating subpackets behave in many respects as solitonlike objects. The analogy with Airy beams is conspicuous.

One can gain additional insights into the nature of the SIP through the current probability $j = i\hbar/2m_1(\psi^*\partial_x\psi - \psi\partial_x\psi^*)$, cf. Fig. 3(f), where the packet is plainly seen to alternate backward and forward net flows. Alternatively, considering the wavelet transform (WT) [41] $\mathbb{W}_{a,b}(\psi) = (1/\sqrt{|a|})\int_{-\infty}^{+\infty}\psi(x)\mathcal{G}^*[(x-b)/a]\mathrm{d}x$, in our case, of the Gabor wavelet family $\mathcal{G}(z) = \sqrt[4]{\pi}\exp(i\omega x)\exp(-x^2/2)$, allows us to decompose the wave function into Gaussian packets, which are the basic packets as far as propagation and diffusion are concerned. This extension of the Fourier transform is common in signal processing but has found so far little echo to study wave packet dynamics [42]. We show in Fig. 3(i) the energy density $|\mathbb{W}_{k,x}|^2$ of the wave function in the $(x-k)$ plane at $t = 100$ ps. One can see clearly how self-interferences confine the polariton packet within the diffusion cone (blue dashed lines) by diverting the flow backward, (i) one or (j) two times when the second inflection point i_2 is reached. Other fundamental connections can be established. For instance, patterns strikingly similar to Fig. 3(e) were observed in the quenched dynamics of a quantum spin chain with magnons [43], a completely different system. This suggests that coupled light fields feature fundamental and universal dynamical evolutions. Combining this characteristic pattern with that of Rabi oscillations leads to the spacetime propagation presented in Fig. 3(k). The protected area exhibits simple Rabi oscillations. The outer area is propagating upper polaritons and is not affected either by oscillations nor interferences. In the SIP area, however, sitting between the two mass walls, the interplay of Rabi oscillations and self-interferences produces a hexagonal lattice. Such a structure is known to arise from interferences of three beams [44,45] and indeed in our case, it arises from interferences of two LPs (on both sides of the inflection point) and one UP [34]. This remarkable structure is, again, sculpted self-consistently out of a unique photon field with a simple Gaussian shape by the dynamics of coupled noninteracting fields. Here, instead of the emergence of propagating particles, a spacetime crystal is formed with the manifest ordering of the previously freely propagating train of polaritons.

In conclusions, we discussed the intricate wave packet propagation of coupled fields (polaritons). Unlike the eventual complete indeterminacy of Schrödinger wave packets in a parabolic dispersion, polaritons can sustain traceable objects with always well-defined properties, such as their shape, position, momentum, and quantum state. This gives rise to a concept of particles similar to that brought by solitons in nonlinear media or Airy beams in noninteracting ones. While these are formed by self-interaction and phase shaping, the individuality of polaritons is acquired and maintained through self-interferences powered by the Rabi coupling. This shows that even in the linear regime, the polariton dynamics is rich and able to produce complex structures out of mere Gaussian initial states. This could lead to applications, following the spirit

of self-accelerating beams. For instance in the classical regime, in a way similar to particle clearing through Airy wave packets [46], polaritons could impart momentum powered by the Rabi oscillations, or, by exciting polaritons with quantum light [47], quantum SIP could propagate in properly wired polariton circuits to perform Linear optical quantum computing, thanks to the linearity of the effect. SIP can indeed carry qubit states at the one-particle level, unlike solitons with which they otherwise share similar propagation qualities.

This work is funded by the "POLAFLOW" ERC Project No. 308136. We thank L. Dominici, D. Ballarini, E. del Valle, and D. Sanvitto for discussions.

*Corresponding author.
fabrice.laussy@gmail.com

[1] T.-K. Ng, *Introduction to Classical and Quantum Field Theory* (Wiley, New York, 2009).
[2] E. Schrödinger, Der stetige übergang von der Mikro- zur Makromechanik, Naturwissenschaften **14**, 664 (1926).
[3] D. J. Korteweg and G. de Vries, On the change of form of long waves advancing in a rectangular canal, and on a new type of long stationary waves, Philos. Mag. B **39**, 422 (1895).
[4] M. V. Berry and N. L. Balazs, Nonspreading wave packets, Am. J. Phys. **47**, 264 (1979).
[5] J. Broky, G. A. Siviloglou, A. Dogariu, and D. N. Christodoulides, Self-healing properties of optical Airy beams, Opt. Express **16**, 12880 (2008).
[6] G. A. Siviloglou, J. Broky, A. Dogariu, and D. N. Christodoulides, Observation of Accelerating Airy Beams, Phys. Rev. Lett. **99**, 213901 (2007).
[7] N. Voloch-Bloch, Y. Lereah, Y. Lilach, A. Gover, and A. Arie, Generation of Electron Airy beams, Nature (London) **494**, 331 (2013).
[8] P. Zhang, Y. Hu, T. Li, D. Cannan, X. Yin, R. Morandotti, Z. Chen, and X. Zhang, Nonparaxial Mathieu and Weber Accelerating Beams, Phys. Rev. Lett. **109**, 193901 (2012).
[9] A. Kavokin, J. J. Baumberg, G. Malpuech, and F. P. Laussy, *Microcavities*, 2nd ed. (Oxford University Press, New York, 2011).
[10] D. Gerace and L. C. Andreani, Quantum theory of exciton-photon coupling in photonic crystal slabs with embedded quantum wells, Phys. Rev. B **75**, 235325 (2007).
[11] J. Kasprzak *et al.*, Bose–Einstein condensation of exciton polaritons, Nature (London) **443**, 409 (2006).
[12] D. Sanvitto, A. Amo, F. P. Laussy, A. Lemaître, J. Bloch, C. Tejedor, and L. Viña, Polariton condensates put in motion, Nanotechnology **21**, 134025 (2010).
[13] I. A. Shelykh, Y. G. Rubo, G. Malpuech, D. D. Solnyshkov, and A. Kavokin, Polarization and Propagation of Polariton Condensates, Phys. Rev. Lett. **97**, 066402 (2006).
[14] A. Amo *et al.*, Collective fluid dynamics of a polariton condensate in a semiconductor microcavity, Nature (London) **457**, 291 (2009).
[15] T. C. H. Liew, Y. G. Rubo, and A. V. Kavokin, Exciton-polariton oscillations in real space, Phys. Rev. B **90**, 245309 (2014).
[16] D. Ballarini, M. De Giorgi, E. Cancellieri, R. Houdré, E. Giacobino, R. Cingolani, A. Bramati, G. Gigli, and D. Sanvitto, All-optical polariton transistor, Nat. Commun. **4**, 1778 (2013).
[17] T. Espinosa-Ortega and T. C. H. Liew, Complete architecture of integrated photonic circuits based on AND and NOT logic gates of exciton polaritons in semiconductor microcavities, Phys. Rev. B **87**, 195305 (2013).
[18] I. Carusotto and C. Ciuti, Quantum fluids of light, Rev. Mod. Phys. **85**, 299 (2013).
[19] O. A. Egorov, D. V. Skryabin, A. V. Yulin, and F. Lederer, Bright Cavity Polariton Solitons, Phys. Rev. Lett. **102**, 153904 (2009).
[20] M. Sich, D. N. Krizhanovskii, M. S. Skolnick, A. V. Gorbach, R. Hartley, D. V. Skryabin, E. A. Cerda-Méndez, K. Biermann, R. Hey, and P. V. Santos, Observation of bright polariton solitons in a semiconductor microcavity, Nat. Photonics **6**, 50 (2012).
[21] H. Flayac, D. D. Solnyshkov, and G. Malpuech, Oblique half-solitons and their generation in exciton-polariton condensates, Phys. Rev. B **83**, 193305 (2011).
[22] G. Christmann, G. Tosi, N. G. Berloff, P. Tsotsis, P. S Eldridge, Z. Hatzopoulos, P. G. Savvidis, and J. J. Baumberg, Oscillatory solitons and time-resolved phase locking of two polariton condensates, New J. Phys. **16**, 103039 (2014).
[23] D. V. Vishnevsky, H. Flayac, A. V. Nalitov, D. D. Solnyshkov, N. A. Gippius, and G. Malpuech, Skyrmion Formation and Optical Spin-Hall Effect in an Expanding Coherent Cloud of Indirect Excitons, Phys. Rev. Lett. **110**, 246404 (2013).
[24] T. Jacqmin, I. Carusotto, I. Sagnes, M. Abbarchi, D. D. Solnyshkov, G. Malpuech, E. Galopin, A. Lemaître, J. Bloch, and A. Amo, Direct Observation of Dirac Cones and a Flatband in a Honeycomb Lattice for Polaritons, Phys. Rev. Lett. **112**, 116402 (2014).
[25] H. Terças, H. Flayac, D. Solnyshkov, and G. Malpuech, Non-Abelian Gauge Fields in Photonic Cavities and Photonic Superfluids, Phys. Rev. Lett. **112**, 066402 (2014).
[26] N. S. Voronova, A. A. Elistratov, and Y. E. Lozovik, Detuning-Controlled Internal Oscillations in an Exciton-Polariton Condensate, Phys. Rev. Lett. **115**, 186402 (2015).
[27] P. Cilibrizzi, H. Ohadi, T. Ostatnicky, A. Askitopoulos, W. Langbein, and P. Lagoudakis, Linear Wave Dynamics Explains Observations Attributed to Dark Solitons in a Polariton Quantum Fluid, Phys. Rev. Lett. **113**, 103901 (2014).
[28] A. Nalitov, D. Solnyshkov, and G. Malpuech, Polariton $\mathbb{Z}$ Topological Insulator, Phys. Rev. Lett. **114**, 116401 (2015).
[29] T. Karzig, C.-E. Bardyn, N. H. Lindner, and G. Refael, Topological polaritons, Phys. Rev. X **5**, 031001 (2015).
[30] T. Espinosa-Ortega and T. Liew, Perceptrons with Hebbian Learning Based on Wave Ensembles in Spatially Patterned Potentials, Phys. Rev. Lett. **114**, 118101 (2015).
[31] L. Dominici *et al.*, Ultrafast Control and Rabi Oscillations of Polaritons, Phys. Rev. Lett. **113**, 226401 (2014).

[32] I. L. Garanovich, S. Longhi, A. A. Sukhorukova, and Y. S. Kivshar, Light propagation and localization in modulated photonic lattices and waveguides, Phys. Rep. **518**, 1 (2012).

[33] S. C. Huang, M. Kato, E. Kuramochi, C. P. Lee, and M. Notomi, Time-domain and spectral-domain investigation of inflection-point slow-light modes in photonic crystal coupled waveguides, Opt. Express **15**, 3543 (2007).

[34] See Supplemental Material at http://link.aps.org/supplemental/10.1103/PhysRevLett.116.026401 for additional analytical and numerical results on polariton propagation, possible implementations in realistic and dissipative systems, 2D cases and descriptions of movies.

[35] G. I. Márk, Analysis of the spreading Gaussian wavepacket, Eur. Phys. J. direct B **18**, 247 (1997).

[36] J. Larson, J. Salo, and S. Stenholm, Effective mass in cavity QED, Phys. Rev. A **72**, 013814 (2005).

[37] C. Antón, T. C. H. Liew, J. Cuadra, M. D. Martín, P. S. Eldridge, Z. Hatzopoulos, G. Stavrinidis, P. G. Savvidis, and L. Viña, Quantum reflections and shunting of polariton condensate wave trains: Implementation of a logic AND gate, Phys. Rev. B **88**, 245307 (2013).

[38] O. Egorov, A. Gorbach, F. Lederer, and D. Skryabin, Two-Dimensional Localization of Exciton Polaritons in Microcavities, Phys. Rev. Lett. **105**, 073903 (2010).

[39] M. Sich *et al.*, Effects of Spin-Dependent Interactions on Polarization of Bright Polariton Solitons, Phys. Rev. Lett. **112**, 046403 (2014).

[40] M. Wimmer, A. Regensburger, C. Bersch, M.-A. Miri, S. Batz, G. Onishchukov, D. N. Christodoulides, and U. Peschel, Optical diametric drive acceleration through action–reaction symmetry breaking, Nat. Phys. **9**, 780 (2013).

[41] L. Debnath and F. A. Shah, *Wavelet Transforms and Their Applications*, 2nd ed. (Birkhäuser, Springer, Basel, 2015).

[42] C. H. Baker, D. A. Jordan, and P. M. Norris, Application of the wavelet transform to nanoscale thermal transport, Phys. Rev. B **86**, 104306 (2012).

[43] W. Liu and N. Andrei, Quench Dynamics of the Anisotropic Heisenberg Model, Phys. Rev. Lett. **112**, 257204 (2014).

[44] T. C. H. Liew, Y. G. Rubo, and A. V. Kavokin, Generation and Dynamics of Vortex Lattices in Coherent Exciton-Polariton Fields, Phys. Rev. Lett. **101**, 187401 (2008).

[45] C. Becker, P. Soltan-Panahi, J. Kronjäger, S. Dörscher, K. Bongs, and K. Sengstock, Ultracold quantum gases in triangular optical lattices, New J. Phys. **12**, 065025 (2010).

[46] J. Baumgartl, M. Mazilu, and K. Dholakia, Optically mediated particle clearing using Airy wavepackets, Nat. Photonics **2**, 675 (2008).

[47] J. C. López Carreño, C. Sánchez Muñoz, D. Sanvitto, E. del Valle, and F. Laussy, Exciting Polaritons with Quantum Light, Phys. Rev. Lett. **115**, 196402 (2015).

Self-Interfering Wave Packets
Supplementary Material

David Colas[1] and Fabrice P. Laussy[2,1,*]

[1]*Departamento de Física Teórica de la Materia Condensada and Condensed Matter Physics Center (IFIMAC), Universidad Autónoma de Madrid, E-28049 Madrid, Spain*

[2]*Russian Quantum Center, Novaya 100, 143025 Skolkovo, Moscow Region, Russia*

I. INTRODUCTION AND OUTLOOK

The theoretical model describing self-interfering wave packets (SIP) is simple: two coupled 1D Schrödinger equations in the linear regime (see section VII for the 2D case). The simplicity of the equation is no guarantee that its extent and depth are rapidly exhausted, as illustrated by the Schrödinger equation, one of the most fundamental equation of modern physics, for which the self-accelerating solution was discovered only in 1979. There should be hope, however, that some closed-form solutions are available. In Section III we show that the SIP, if it has such analytical expressions, does not seem to be reducible to a simple closed form. We could express it as a complex combinatorial superposition of Bessel functions, as could be expected from propagating packets, weighted by polaritonic factors, such as the dressed momentum k_Ω. Before discussing this structure, we start in Section II with more details on the exact solutions, both from the formalism and numerical simulations point of view, contrasting in particular the multitude of ways that one has to poke at the polariton wave function. Following Sections mainly consider the impact of some complications found in actual setups. In Section IV, we discuss some possible tricks to help shaping the SIP in cases narrow-enough pulses cannot be readily implemented in the laboratory. In Section V, we consider the impact of finite lifetimes. In Section VI, we provide supplementary information on the spacetime crystal. Last Section, VIII, gives an overview of the rest of the Supplementary Material, that consists of animated movies that illustrate, maybe better than equations, the mesmerizing dynamics of polaritons.

II. MORE POLARITON PROPAGATION

The polariton propagator, Eq. (1) of the main text [1] is easily found in k space (we work here with $\Delta = 0$):

$$\langle k'|\Pi|k\rangle = \begin{pmatrix} \exp(\frac{-ik^2 m_+ t}{4})\left(\cos(\frac{k_\Omega^2 t}{4}) + i\frac{k^2}{k_\Omega^2} m_- \sin(\frac{k_\Omega^2 t}{4})\right) & -\frac{i4\Omega_{\rm R}}{k_\Omega^2}\exp(\frac{-ik^2 m_+ t}{4})\sin(\frac{k_\omega^2 t}{4}) \\ -\frac{i4\Omega_{\rm R}}{k_\Omega^2}\exp(\frac{-ik^2 m_+ t}{4})\sin(\frac{k_\omega^2 t}{4}) & \exp(\frac{-ik^2 m_+ t}{4})\left(\cos(\frac{k_\Omega^2 t}{4}) - i\frac{k^2}{k_\Omega^2} m_- \sin(\frac{k_\Omega^2 t}{4})\right) \end{pmatrix} \delta(k-k')\,, \tag{S1}$$

where we remind the important dressed momentum variable k_Ω:

$$k_\Omega \equiv \sqrt[4]{k^4 m_-^2 + 16 m_+^2 \Omega_{\rm R}^2}\,, \tag{S2}$$

with $m_\pm = (m_{\rm C} \pm m_{\rm X})/(m_{\rm C} m_{\rm X})$ (note again that k_Ω is a function of k). We also assume $\hbar = 1$. Polaritons are maybe best formally defined as the states with a well-defined momentum and, consequently, also energy. They satisfy:

$$\Pi(t)\,\|k\rangle\rangle_\pm = \exp(-iE_\pm t)\,\|k\rangle\rangle_\pm\,, \tag{S3}$$

and as such are expressed as:

$$\|k\rangle\rangle_\pm \propto \begin{pmatrix} E_\pm(k) \\ 1 \end{pmatrix}|k\rangle\,, \tag{S4}$$

for $+$ (resp. $-$) the upper (resp. lower) polariton, with $E_\pm$ the pivotal polariton quantity, the dispersion:

$$E_\pm = k^2 m_+ \mp k_\Omega^2\,. \tag{S5}$$

States (S4) form a canonical basis out of which a general polariton state is obtained by linear combination:

$$\|\psi\rangle\rangle_\pm = \int_{-\infty}^{\infty} \phi_\pm(k)\,\|k\rangle\rangle_\pm\, dk\,, \tag{S6}$$

with $\phi_\pm(k)$ the scalar-field (upper/lower) polariton wave function. All the results in this text follow from the impossibility to evolve such a general polariton state in time with the complex rotation of free propagation as in Eq. (S3), due to its two-component character. We have already discussed in the main text some important constrains of such a structure: for instance, that except for a well-defined polariton state in k space, i.e., a completely delocalized polariton in real space, the photon and exciton components of a polariton cannot be jointly defined according to a given wave packet $\phi(k)$, e.g., a Gaussian packet, since one component gets modulated by the $E_\pm$ factor needed to maintain the particle on its branch. Gaussian packets for both the photon and the exciton result in populating both polariton branches. The general case obviously admixes the two types of polaritons:

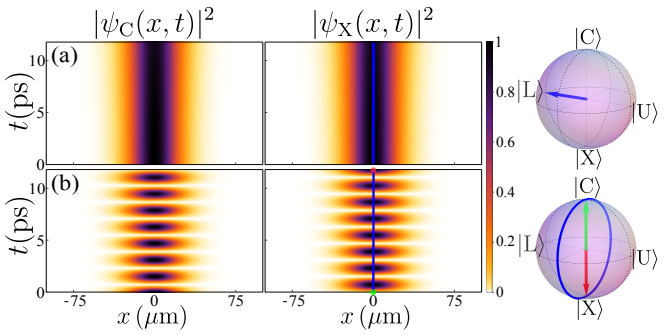

FIG. 1: (Color online) Polariton propagation of delocalized wave packets, as seen through the photonic (ψ_C) and excitonic (ψ_X) components for the cases of (a) upper row: a lower polariton at $t = 0$ and (b) lower row: a photon. The diffusion is negligible over the selected time window and the staggering on the dispersion too small to evidence polariton self-interference effects. Parameters: $\Omega_R = 2$ meV, $m_C = 0.025$ meV ps^2 μm^{-2}, $m_X = 2$ meV ps^2 μm^{-2}, $\sigma_x = 20$ μm.

$|\psi\rangle = \sum_{\sigma=\pm} \int \phi_\sigma(k) \, ||k\rangle\rangle_\pm \, dk$. These results that impose strong constrains on a polariton wave packet must be contrasted with the conventional picture one has of the polariton as a particle, which is that of states $||k\rangle\rangle_\pm$ and is, in good approximation, recovered for large enough packets as shown in Fig. 1. The particle is here broad enough in space to have a small diffusion, cf. Eq. (2), and Rabi oscillations may be present depending on the state preparation, which however does not result in qualitative novelties. The situation is completely different when considering a spread of the wave function in k space, that is, sharp packets in real space. The propagation of such sharp packets is shown in Fig. 2 for various initial conditions: as a lower polariton (left part of the figure) or as a bare particle (exciton or photon, right part of the figure) and such that the excitonic component is perflectly localized at $t = 0$ (upper row) or the photon component is (lower row). The wave packet evolution is also shown as seen either through its photon or exciton field. Experimentally, the photon field is typically the one observed by recording the light leaked by the cavity. One sees variations around the themes exposed in the main text, with more or less pronounced features in some of the configurations. The clearest effects are obtained for confined excitons, and observation through the cavity is always a good vantage point. For each case of propagation in space-time, we also show in Fig. 2(α–η) the corresponding dispersion, which is the double Fourier transform (over space and time). This shows how, indeed, the lower polariton only populates its own branch. It also provides an alternative view of the various localized states, e.g., the localized photon does not populate the photon-like part of the polariton branch in the exciton spectrum (panel δ) and vice-versa with the localized exciton in the photon spectrum (panel α).

We now proceed with the underlying mathematical expressions. For, say, the lower polariton case prepared so that the photon component is perfectly localized at $t = 0$ (in the case where, for concision in the notation, we assume from now on $m_X \to \infty$), we find from Eqs. (S1–S6):

$$\psi_C(k,t) = \exp\left(-i\frac{k^2 - k_\Omega^2}{4m_C}t\right)\frac{k_\Omega^2 - k^2}{4\Omega_R m_C}, \quad \text{(S7a)}$$

$$\psi_X(k,t) = \exp\left(-i\frac{k^2 - k_\Omega^2}{4m_C}t\right). \quad \text{(S7b)}$$

The result is extremely simple in this picture (time–momentum). There is no time dynamics for the density $|\psi_{X,C}|^2$: the perfectly localized exciton at $t = 0$ results in a completely delocalized wave function at all times $|\psi_X|^2 = 1$. The corresponding photon wave function is qualitatively similar to a Voigt lineshape in k space, which we will use in next Section to derive approximate expressions. It is shown on the left column of Fig. 3. In all cases, however, there is of course a dynamics of the wave function itself, as seen through its real and imaginary parts on the figure. There is a slowing down of the oscillations with increasing $|k|$. The Fourier transform in k of this pattern gives the spacetime propagation in Fig. 2(a).

The case of a perfectly localized exciton as the initial condition (i.e., in the photon vacuum rather than the field needed to provide a lower polariton), i.e., $\psi_-(x, t = 0) = (\delta(x), 0)^T$, is given directly by the columns of Eq. (S1):

$$\psi_C(k,t) = \exp\left(-\frac{ik^2t}{4m_C}\right)\left[\cos\left(\frac{k_\Omega^2 t}{4m_C}\right) - i\left(\frac{k}{k_\Omega}\right)^2 \sin\left(\frac{k_\Omega^2 t}{4m_C}\right)\right], \quad \text{(S8a)}$$

$$\psi_X(k,t) = \exp\left(-\frac{ik^2t}{4m_C}\right)(-i\Omega_R t)\,\mathrm{sinc}\left(\frac{k_\Omega^2 t}{4m_C}\right). \quad \text{(S8b)}$$

The corresponding propagation in the momentum space is shown on the right column of Fig. 3. There is, this time, a dynamic in the density, namely, the Rabi oscillations, with now a speeding up of the oscillations with increasing $|k|$, corresponding to the effective Rabi frequency of effectively detuned exciton-photon coupled states. The Fourier transform in k of this pattern gives the spacetime propagation in Fig. 2(e).

We have also discussed in the main text how a polariton wave packet propagates with a group velocity $v_\pm = \partial_k E_\pm(k)$ that, for the lower polariton, features a local maximum. It

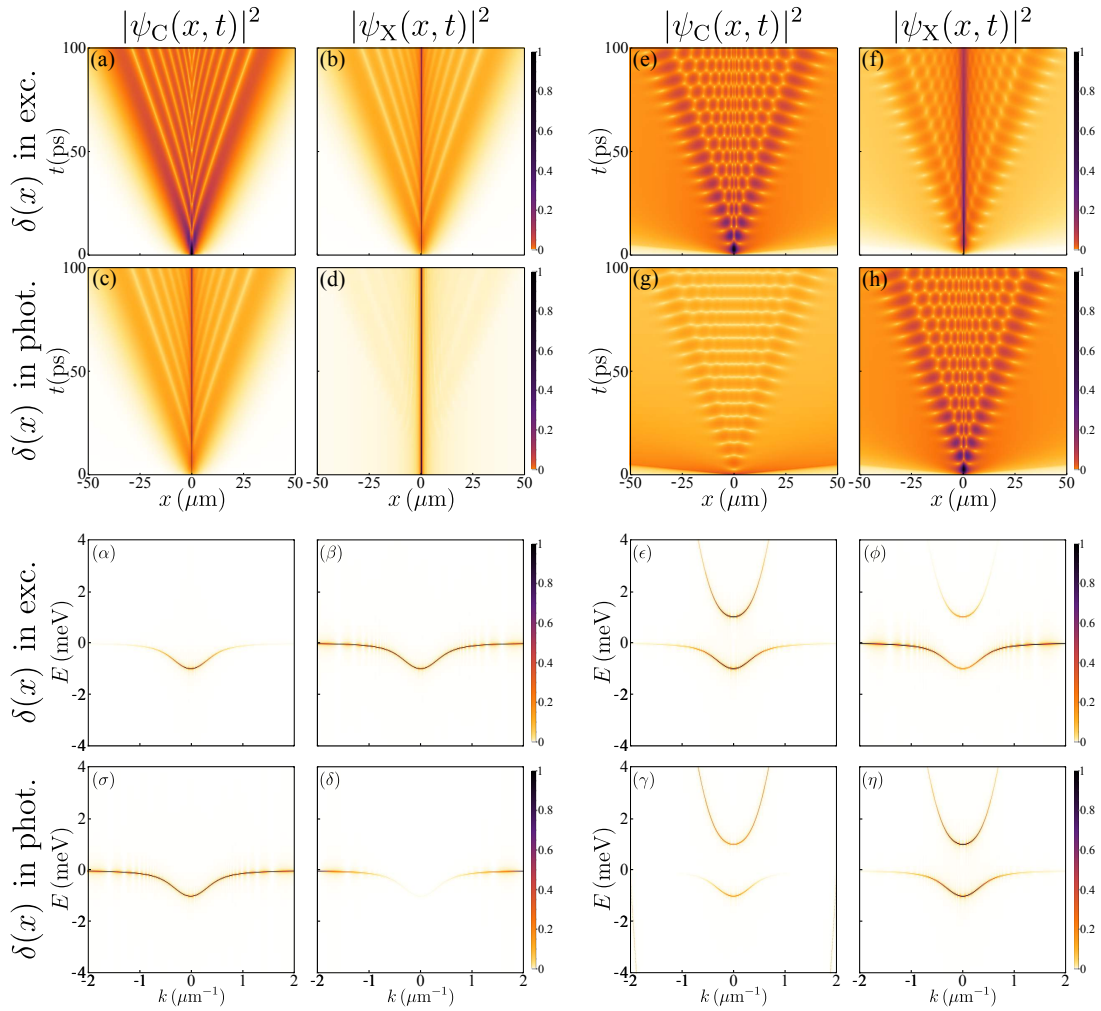

FIG. 2: (Color online) Propagation of sharp packets. As seen in both real space as a function of time (upper two rows) and through their dispersion (energy as a function of momentum, lower two rows) through the light emitted by the cavity (C) or through the direct exciton emission (X) for the cases of a lower polariton propagation (two columns on the left) and of a bare state propagation (two columns on the rigth). In the case of polaritons, (a–d), the exciton (upper row) or the photon (lower row) is perfectly localized at $t = 0$ with the other component defined such that the the particle remains on its branch. In the case of bare particles (e–h), the initial state is simply a photon (upper row) or an exciton (lower row) with the other component empty at $t = 0$. Greek-numbered panels correspond to the latin-numbered ones. Parameters: $\Omega_R = 0.5$ meV, $m_C = 0.5$ meV ps^2 μm^{-2}.

reads:

$$v_- = \frac{k}{2m_+} - \frac{\frac{\Delta}{k} - \frac{k}{2m_-}}{\sqrt{1 - \frac{4m_-\Delta}{k^2} + \frac{4m_-^2(4\Omega_R^2+\Delta^2)}{k^4}}}, \qquad \text{(S9)}$$

which is shown in Fig. 4 (blue line). The local maximum is obtained at the first inflection point of the dispersion, $k = i_1$, where the polaritons also do not diffuse. Increasing the momentum makes the particle heavier and actually reduces its speed. A local minimum is attained at the second inflection point, $k = i_2$, where the polariton also propagate without diffusion but now with a low speed. At larger k, Eq. (S9) becomes linear and tends to the speed of the bare exciton, as indeed for $k \gg 0$, $v_-(k) \to k/m_X$, cf. Fig. 4 in dashed red for a non detuned system. If there is no second inflection point (for an infinitely heavy exciton mass), there is an absolute maximum speed for the polaritons since the bare exciton group velocity vanishes (green curve).

III. APPROXIMATIONS

We could not find manageable closed form expressions for the Fourier transform of the term $\exp(k_\Omega^2 - k^2)$. The representation of this term in real space captures the (lower) polaritonic self-interference effect. The term $k^2 - k_\Omega^2$ for the (lower) polariton momentum distribution can however be well approximated by a Voigt distribution, since it combines both exponential and fat-tail types of decay. Since the fat-tail could be expected to play a dominant role qualitatively, we assume simply a Lorentzian distribution $f(k) = 4\Omega_R m_C/\left(1 + \frac{k^2}{4\Omega_R m_C}\right)$,

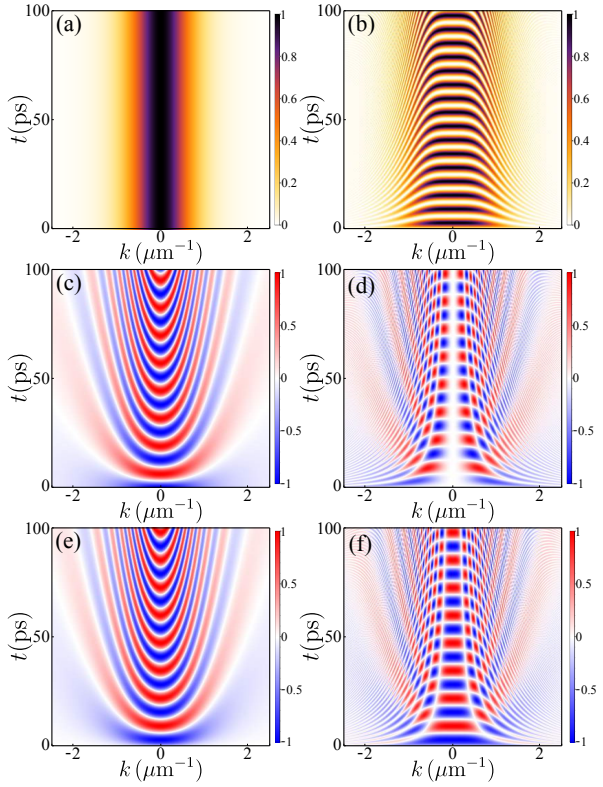

FIG. 3: (Color online) Propagation in k space for non-diffusing packets of, left column, a lower polariton and, right column, a photon, as seen through, from up to bottom: $|\psi_{\rm C}(k,t)|^2$, $\Re(\psi_{\rm C}(k,t))$ and $\Im(\psi_{\rm C}(k,t))$. Parameters: $\Omega_{\rm R} = 0.5$ meV, $m_{\rm C} = 0.5$ meV ps^2 μm^{-2}.

thus approximating Eq. (S7b) by:

$$\psi_{\rm X}(k,t) \simeq \frac{-\exp\frac{it\Omega_{\rm R}}{1+k^2/(4m_{\rm C}\Omega_{\rm R})}}{1+k^2/(4m_{\rm C}\Omega_{\rm R})}\,, \qquad \text{(S10)}$$

which Fourier Transform can be obtained by a series expansion of the exponential, providing the real space dynamics of the SIP:

$$\psi_{\rm X}(x,t) \simeq \sum_{n=0}^{\infty} \frac{-4\sqrt{\pi}(m_{\rm C}\Omega_{\rm R})^{\frac{3+2n}{4}}(it\Omega_{\rm R})^n|x|^{\frac{1}{2}+n}K_\alpha(2\sqrt{\Omega_{\rm R}m_{\rm C}}|x|)}{n!^2}\,, \qquad \text{(S11)}$$

where $K_\alpha(z)$ is the modified Bessel function (solution of th equation $z^2y''+zy'-(z^2+n^2)y=0$) and with $\alpha = n+1/2$. The propagation of the wave packet calculated numerically with the Fourier Transform (a) and the one obtain with the analytical formula in Eq. S11 (b) are compared in Fig. 5. There is a good qualitative agreement, with only the size of the propagation cone differing slightly, due to the width difference between the Lorentzian distribution and the actual one. One can therefore trust the approximation to give some insights into

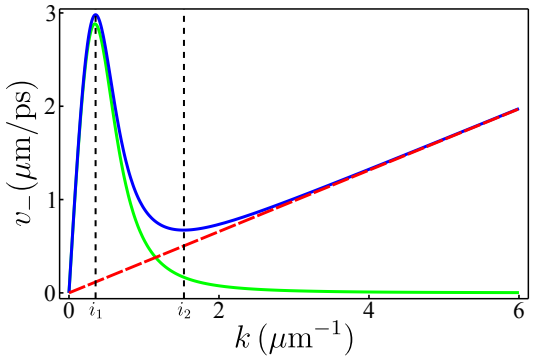

FIG. 4: (Color online) Speed of the lower polariton as a function of its imparted momentum: there is a maximum and larger momenta result in slower particles. Local maxima are given by the inflection points. At large enough k, the polariton becomes exciton-like and suffers no such restriction. If the exciton mass is infinite, polaritons have an absolute maximum velocity.

the nature of the SIP. First, the SIP is indeed a phenomenon of many interferences. The convergence of the series is obtained for a number of terms in the sum that increases linearly with time t, showing how each new peak arises from an added term and thus a next order in the interference. Also, at the center of the wave packet ($x = 0$), the previous expression can be reduced to a simple form:

$$\psi_{\rm X}(x=0,t) \simeq -2\pi\sqrt{\Omega_{\rm R}m_{\rm C}}\,{\rm e}^{\frac{it\Omega_{\rm R}}{2}}\,J_0\left(\frac{t\Omega_{\rm R}}{2}\right)\,, \qquad \text{(S12)}$$

where $J_n(z)$ is the Bessel function of the first kind. Since the departure between Eq. (S11) and the exact numerical solution is mainly due to the extent of the envelope of the momentum, one can expect a better agreement at $x = 0$, and indeed we find that there is a perfect match, as seen in Fig. 5(c). Equation (S12) confirms that the successive peaks that shape the SIP appear at the Rabi frequency $\Omega_{\rm R}$. The photon mass $m_{\rm C}$ (we remind that we assumed here an infinite exciton mass) acts only on the intensity. In the same way, one can obtain the corresponding series for the photon field:

$$\psi_{\rm C}(x,t) \simeq \sum_{n=0}^{\infty} \frac{4\sqrt{\pi}(m_{\rm C}\Omega_{\rm R})^{\frac{2n+1}{4}}(it\Omega_{\rm R})^n|x|^{n-\frac{1}{2}}K_\beta(2\sqrt{\Omega_{\rm R}m_{\rm C}}|x|)}{n!\Gamma(n)}\,, \qquad \text{(S13)}$$

with $\beta = n - 1/2$, showing the sort of complexity that describes both structures and how they are tightly related. Series for photons or excitons as initial conditions can also be obtained from Eq. S8a and S8b, involving Hypergeometric functions which, however, are too cumbersome to be written here.

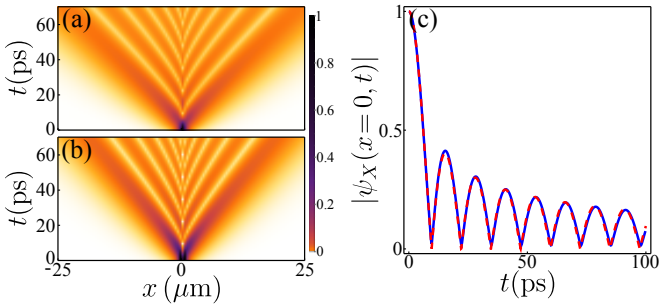

FIG. 5: (Color online) (a,b) $|\psi_{\rm X}(x,t)|^2$ calculated from the exact result Eq. (S7b) and the approximated one, Eq. (S11). (c) Normalized intensity at the center of the wave packet ($x = 0$): exact result through the Fourier Transform of Eq. (S7b) (blue line) and the analytical expression Eq. (S12) (red dashed line). The approximation appears to be exact at $x = 0$.

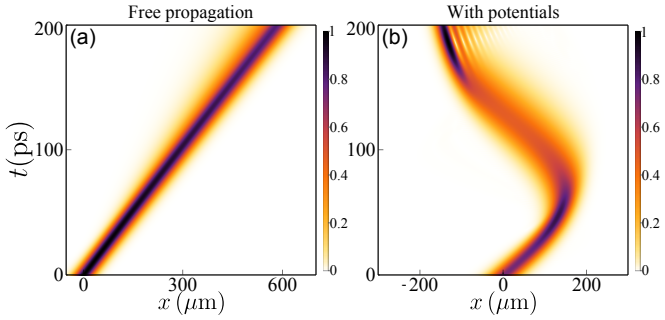

FIG. 6: (Color online) SIP within a harmonic potential. A polariton wave packet with width $\sigma_x = 20$ µm imparted with a momentum $k_0 = i_1$ and (a) propagating freely or (b) within a harmonic potential.

IV. SHAPING A SIP BY COLLIDING A GAUSSIAN PACKET ON A POTENTIAL

We have shown that a SIP can be obtained by self-shaping out of a freely propagating polariton Gaussian wave packet. This is achieved by starting with a narrow enough packet in real space to obtain the largest spread in the Fourier space. This involves two physical limits: the size of the laser spot and the effective mass of the particles. For the former, one needs to reduce as much as possible the size of the laser spot, which is experimentally limited by the laser's wavelength (in a good approximation). For the latter, smaller masses of the cavity photon and of the exciton result in steeper dispersions. This allows to observe the SIP with a smaller breadth of ks, in addition to setting the inflexion points closer to $k = 0$. These are parameters that can be played with experimentally. Conceivably, one can even turn to different objects such as light-hole excitons, or different platforms, such as photonic crystal slabs (PhCs) with embedded quantum wells [10], to reach a regime of polaritons with comparable masses. Indeed, PhCs can provide a better field confinement and thus lead to stronger polaritonic effects on various modes with the appearance of so-called *photonic crystal polaritons*. If, however, one is unwilling or unable to achieve the SIP regime in this way, it is possible to enforce it by involving external factors. For illustration, we show how to squeeze the packet in space by bouncing it off a potential wall, increasing *de facto* its spread in k space. In Fig. 6, we show the propagation of a polariton wave packet in the presence of harmonic potentials $V(x) = \frac{1}{2} m_{\rm C,X} \omega_{\rm C,X}^2 x^2$ for the photonic/excitonic fields, with $\omega_{\rm C,X} = \hbar/(m_{\rm C,X}\sigma^2)$. While the free propagation of a broad packet ($\sigma_x = 20$ µm) does not exhibit interferences (a), the staggering on the branch being too small, the same packet propagated inside the potentials squeezes as it bounces back one wall and then develops self-interferences (b), the squeezing reducing the packet size in space, thereby increasing its spread on the branch on either side of the inflection point. Essentially the same result is obtained with only the photonic potential. Switching it off would allow to free the SIP into free propagation.

V. SIP IN DISSIPATIVE SYSTEMS

So far, we have only considered conservative situations. Polaritons are however particles with a finite lifetime, which allows their continuous observation. A careful study of the main sources of decay and dephasing for polaritons has been presented before (ref. [31] of the main text), estimating the photon lifetime as $\gamma_{\rm C} \simeq 5$ ps, while the exciton lifetime is much larger $\gamma_{\rm X} \simeq 1$ ns. Therefore, we only consider here the photon lifetime, adding in the first matrix element of the polariton propagator (see Eq. (1)) the quantity $-i/\gamma_{\rm C}$. In Fig. 7, we show the propagation of a lower polariton wave packet, similar to the case in Fig. 3(e) of the main text, but this time including the photon lifetime ($\gamma_{\rm C} = 5$ ps). The self interferences are still visible till around ten times this lifetime and then vanish. This is due to the fact that photon-like polaritons (small k components) are more damped than the exciton-like ones (high k components) and with one part of the overlapping wave function gone, the self-interference disappears. This can be observed on Fig. 7(d) with the wavelet transform of the wave function at $t = 100$ ps. At this time, one can see that only the high k components remain ($|k| > i_1$), where the polaritons are strongly excitonic. It can also be seen through the evolution of the quantum state in this region (cf. the Bloch sphere in panel (c)), converging to the $|{\rm X}\rangle$ state. Unlike the non dissipative case (Fig. 3(i) of the main text), in the diffusion cone, the packet is then only composed of a single k component whereas at least two different k components are needed to obtain self-interferences. As a result, the wave function takes a two-peaked shape with a strong depletion of particles at the center, as shown in Fig. 7(c). In contrast, the SIP formed at the second inflection point (cf. Fig. 3(j) of the main text without decay), being excitonic-like on both sides, is much more robust to decay. The interferences persist at all times as shown in Fig. 7(e), since both components around i_2 remain present, as displayed on the scalogramm in panel (f).

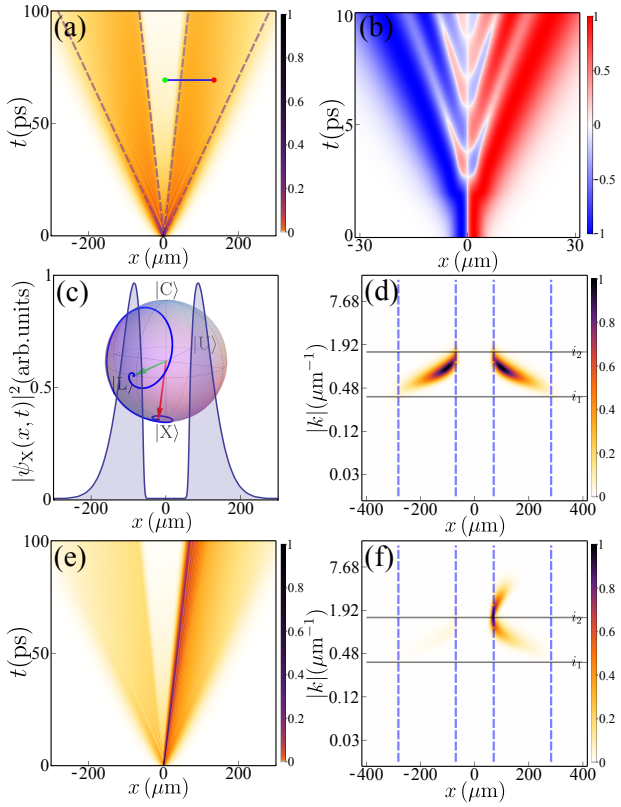

FIG. 7: (Color online) SIP with radiative decay. (a) Propagation of a lower polariton packet with non-zero photon lifetime $\gamma_C = 5$ ps. (b) Current probability j at early times. (c) Intensity profile at $t = 100$ ps with the evolution of the quantum state on the Bloch sphere corresponding to the path (from green to red) plotted in (a). (d) Wavelet decomposition of (a) at $t = 100$ ps. (e-f) Propagation and wavelet decomposition in the same conditions but exciting with a momentum at $k_0 = i_2$. One can see how the SIP disappears when the overlap between k components is lost by radiative decay of the photonic part. The parameters are the one used in Fig. 3 (e-l) of the main text.

VI. HEXAGONAL LATTICE IN SPACE AND TIME

We have shown that the combination of self interferences and Rabi oscillations gives rise to a hexagonal lattice in space and time, cf. Fig. 3(k,l) of the main text. Such a hexagonal structure arises from an interference between three different fields, all emerging from the single photonic field ψ_C. We now describes in more details the nature of this interference. The photonic field is not an eigenstate and exciting the cavity induces Rabi oscillations, that can be seen as the result of beatings between two harmonics (eigenstates): the lower (LP) ψ_- and upper (UP) ψ_+ polaritons. This provides two out of the three beams. As already mentioned, Rabi oscillations occur only if there is a spatial overlap between the two polaritonic fields. For instance, they can be seen in Fig. 8(a) in the central area. If one enters the SIP regime by exciting a large part of the dispersion, the field ψ_- interferes with itself, providing effectively two additional fields in the same spatial area. The diffusion cone thus contains $\psi_-(0 < k < i_1)$

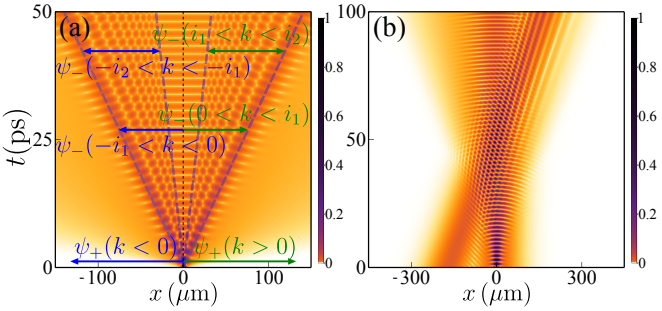

FIG. 8: (Color online) (a) Propagation of a SIP with Rabi oscillations, exhibiting a spacetime hexagonal lattice. Specific areas are identified to explain the effect as the interference of three beams. The different arrows indicate which components of the different fields (ψ_+ and ψ_-) diffuse within these areas. The lattice is formed by two LP fields and one UP field. Rabi oscillations or simple diffusions are obtained in areas with only two and one field, respectively. (b) A hexagonal lattice in space and time can be also produced by making interfering three independent beams: exciting resonantly a lower polariton and an upper polariton (providing Rabi oscillations) produces the same pattern when overlaping with another lower polariton field imparted with a momentum (here with $k_0 > i_1$).

and $\psi_-(i_1 < k < i_2)$ (or symmetrically on the negative k; note also that if the second inflection point is reached, it also contains $\psi_-(k > i_2)$). The field ψ_+ does not suffer from any restriction in its diffusion. On the Fig. 8(a), the three effective fields present within the diffusion cone are delimited by green arrows (on the right hand side, by blue arrows for their symmetric on the left hand side). In panel (b), we also show that this pattern is formed with three independent fields by creating two polariton beams (upper and lower), by resonant excitation at $k_0 = 0$ (exhibiting Rabi oscillations due to their spatial overlap), on which is sent another lower polariton beam imparted with a momentum $k > i_1$, that gives rise to a hexagonal lattice in the common interference area. In the SIP case, however, all this phenomenology follows self-consistently from a single photon beam. It is also maintained as the packet diffuses instead of occuring only in the region of spatial overlap (a SIP can be however maintained at long times, as seen on the figure).

VII. SIP IN TWO DIMENSIONS

Up to now, we have considered 1D cases, which are indeed possible in heterostructures by confining in the two other dimensions (quantum wires). Polariton propagation is however popular in the 2D geometry as well and we briefly discuss what happens in this case. Since the system is linear and uncoupled in transverse coordinates, the dynamics follows trivially from the previous results and symmetry. With a full radial symmetry, all the phenomenology is conserved in 2D, with rotational invariance. This is shown in Fig. 9(a) where the propagation of a SIP is shown after 100 ps, after preparing a narrow Gaussian wave packet at $t = 0$ (and at the origin of the plane). This is the counterpart of the case of Fig. 3(e)

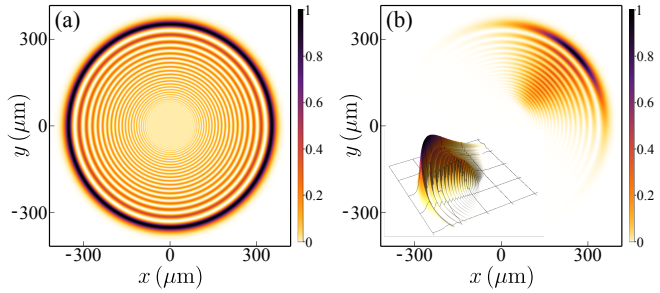

FIG. 9: (Color online) SIP in 2D. (a) With full radial symmetry when self-interfering in all directions. A central disk is shielded from interference like in the 1D case and features a flat plateau of lower polaritons. (b) When imparted with momentum, the packet self-interferes in the direction of its propagation and diffuses radially. Parameters: $\Omega_{\rm R} = 2$ meV, $m_{\rm C} = 0.025$ meV ps^2 μm^{-2}, $m_{\rm X} = 2$ meV ps^2 μm^{-2}, (a) $\sigma_x = 2$ μm, (b) $\sigma_x = 4$ μm, $k_x = k_y = i_1$.

of the main text. The propagation and thus the shape of the wave packet are similarly determined by the dispersion and the way it is excited. There is also, depending on the proximity of the second inflection point, a central area shielded from the interferences, which is now a disk, whose diameter is also determined by a zero of $\partial_k^2 E_- = 0$. Also, like in the 1D case, one can impulse the propagation of the packet in a desired direction by imparting a momentum. This is shown in Fig. 9(b) with the propagation of a smaller wave packet when exciting the dispersion at the first inflection point ($k_x = k_y = i_1$). By using squeezed Gaussian packets, one can propagate a SIP with fronts that remain parallel and orthogonal to the direction of motion.

VIII. MOVIES

We also provide three movies that illustrate vividly the polariton dynamics.

The movie `I-QuantumState.avi` animates Fig. 3(e,h) of the main text. It shows how a narrowly squeezed lower polariton wave packet self-interferes and produces, as a result, two trains of subpackets propagating back to back, emerging from a polariton sea shielded from the interferences. To show how the overall structure of the SIP is connected to the individual identity of each packet, we also present dynamically on the Bloch sphere the evolution of the quantum state on a path that links the center of the wave packet to the side of the diffusion cone (from the green to the red point on the density plot, mached with the green and red arrows on the sphere). The state in the central area—shielded from interferences—is the lower polariton. In the interferences zone, crossing a fringe induces a loop on the sphere that crosses the meridian of states $|\mathrm{C}\rangle$–$|\mathrm{L}\rangle$–$|\mathrm{X}\rangle$. Each peak converges in time towards a well defined polariton state on the meridian.

The movie `II-PolaritonRiffle.avi` animates the case of Fig. 2(d,e) of the main text. It shows the propagation of a photon wave packet (at $t = 0$) with a momentum and negative detuning. A judicious choice of parameters permits to maintain a spatial overlap between the two polaritons, conserving the Rabi oscillations which, due to the detuning, are bent in spacetime (see main text). This results in the propagation of ultrafast subpackets within the mother packet. This is well seen on the animation after 35 ps of animation time, which is the time needed for the packet to develop the structure (the initial condition is a Gaussian packet).

The movie `III-SipPotentials.avi` animates the case of Fig. 6(b). It shows on the left panel the propagation of a large lower polariton wave packet (of $\sigma_x = 20$ μm) imparted with a momentum in the presence of a harmonic potential (in green). On the right panel, the scalogram obtained by the wavelet transform allows to follow dynamically the evolution of the packet in the x–k plane. Such a packet, due to its large size, does not exhibit self-interferences. However, in the presence of the potential, the packet squeezes in real space, as it collides against the potential, and thus extends its spread in the Fourier space. When this causes a superposition between k components below and above the inflection point, as can be seen on the scalogram, the SIP manifests.

---

[1] Equations from the main text are quoted as numbers, those from the Supplementary [this text] are prefixed by "S".